

# Structures and electronic phases of the bis(ethylenedithio)tetrathiafulvalene (BEDT-TTF) clusters and $\kappa$ -(BEDT-TTF) salts: A theoretical study based on *ab initio* molecular orbital methods

Yutaka Imamura,<sup>a)</sup> Seiichiro Ten-no, Kenji Yonemitsu, and Yoshitaka Tanimura

*The Graduate University for Advanced Studies and Institute for Molecular Science, Myodaiji, Okazaki 444-8585, Japan*

(Received 21 April 1999; accepted 9 July 1999)

Electronic and geometrical structures of bis(ethylenedithio)tetrathiafulvalene (BEDT-TTF) molecules are studied using *ab initio* molecular orbital methods. The optimized structure of a BEDT-TTF monomer is close to the experimental one within errors of 0.02 Å and 0.5 deg in bond length and angle, respectively, except the ethylene group. *Ab initio* parameters such as transfer integrals and Coulomb interactions are determined from the BEDT-TTF dimer and tetramer calculations. Using model Hamiltonians with the *ab initio* parameters, we investigate the electronic states based on the exact diagonalization method. The results show that the ground state has antiferromagnetic correlation which is consistent with experimental results. We study the effects of long-range Coulomb interactions employing the 2-D extended Hubbard model with the Hartree–Fock approximation. It is found that the ground state shows various phases; antiferromagnetic, charge ordering, and paramagnetic ones, controlled by the long-range interactions. © 1999 American Institute of Physics. [S0021-9606(99)30437-2]

## I. INTRODUCTION

The organic conductor, TTF-TCNO, synthesized in 1973, gathered much attention because of its high electrical conductivity.<sup>1</sup> Since this discovery, many other organic conductors have been synthesized and studied. One of them, a BEDT-TTF salt, exhibits a high superconducting transition temperature,  $T_c$ . BEDT-TTF shown in Fig. 1 is a donor molecule which produces various kinds of charge transfer crystals classified into  $\alpha$ -,  $\beta$ -,  $\kappa$ -, etc., phases. Among them, the  $\kappa$ -BEDT-TTF salts are composed of two dimensional (2-D) donor sheets in which paired BEDT-TTF molecules are arranged almost orthogonal to each other (see Fig. 2). The formal charges of the BEDT-TTF molecule and the counterion are +1/2 and -1, respectively. The space group of  $\kappa$ -(BEDT-TTF)<sub>2</sub>Cu[N(CN)<sub>2</sub>]X (X=Cl, Br, and I) is Pnma. At ambient pressure, the  $\kappa$ -(BEDT-TTF)<sub>2</sub>Cu[N(CN)<sub>2</sub>]Br salt shows superconductivity below  $T_c = 11.6$  K, whereas  $\kappa$ -(BEDT-TTF)<sub>2</sub>Cu[N(CN)<sub>2</sub>]Cl is a Mott insulator with antiferromagnetic (AF) ordering<sup>2,3</sup> as shown in Fig. 3.<sup>4</sup> However, under 0.3 kbar, the latter becomes a superconductor with  $T_c = 12.8$  K. On the other hand,  $\kappa$ -(BEDT-TTF)<sub>2</sub>Cu[N(CN)<sub>2</sub>]I does not show superconductivity. Electronic properties of the BEDT-TTF salts are therefore very sensitive to pressure and counteranions.

Various theoretical studies have been done for the BEDT-TTF salts.<sup>5–23</sup> From the first-principles approach, Xu *et al.* calculated the Fermi surfaces of  $\kappa$ -(BEDT-TTF)<sub>2</sub>Cu(NCS)<sub>2</sub> using the local density approximation (LDA) based on the density functional theory (DFT).<sup>5</sup> From the *ab initio* molecular orbital (MO) theory,

Demiralp and Goddard optimized the BEDT-TTF monomer at HF/6-31G\*\* and studied the physical properties using the 2-D Hubbard model within the Hartree–Fock (HF) approximation.<sup>6–10</sup> Kino and Fukuyama adopted the same model and explained the different physical properties of  $\kappa$ -(BEDT-TTF)<sub>2</sub>X,  $\alpha$ -(BEDT-TTF)<sub>2</sub>I<sub>3</sub>, and (BEDT-TTF)<sub>2</sub>MHg(SCN)<sub>4</sub> using a couple of key parameters, the band overlap and the dimerization.<sup>11–13</sup> Fortunelli and Painelli described the *ab initio* evaluation of Hubbard parameters for the BEDT-TTF dimer unit of the  $\kappa$ -(BEDT-TTF)<sub>2</sub>Cu[N(CN)<sub>2</sub>]Br salt.<sup>14–17</sup> Okuno and Fukutome showed an effective Hamiltonian of  $\beta$ - and  $\kappa$ -phases and concluded that the electron correlation is very strong.<sup>18</sup> The nesting and pressure effects of the Fermi surface were discussed in Refs. 19 and 20. Using the dimer Hubbard model within the spin fluctuation exchange (FLEX) approximation, the pairing symmetry and the superconducting transition temperature,  $T_c$ , were studied.<sup>21–23</sup>

Although the components of the conductors are organic molecules, to which *ab initio* methods have been successfully applied, there has been no quantitative study of bulk properties based on the *ab initio* MO theory. The purpose of this paper is to clarify the structure and electronic phases of the BEDT-TTF salts started from the *ab initio* MO theory. This will be of great importance for designing organic conductors since their electronic states are very sensitive to constitution and arrangement of organic molecules. Such analyses were made recently for the 1-D dicyanoquinonediimine (DCNQI) salts.<sup>24,25</sup> We first perform *ab initio* MO calculations of BEDT-TTF molecules and study their geometrical and electronic structures. Based on those results, we construct a model Hamiltonian of finite cluster models and calculate electronic states by the exact diagonalization method.

<sup>a)</sup>Electronic mail: ima@ims.ac.jp

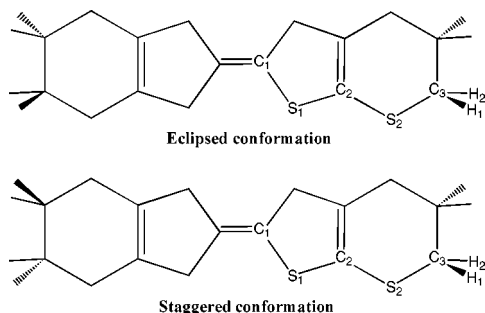


FIG. 1. Molecular structure of the BEDT-TTF molecule.

The obtained electronic phases are analyzed by spin-correlation functions. The previous 2-D Hubbard model calculations included only the on-site Coulomb effects.<sup>9,11–13</sup> However, Seo and Fukuyama, and Kobayashi *et al.* suggested the importance of long-range Coulomb interactions.<sup>26,27</sup> Therefore, we adopt the 2-D extended Hubbard model including long-range as well as on-site Coulomb interactions.

The organization of this paper is as follows. In Sec. II, we discuss geometrical structures and parametrize transfer integrals and Coulomb interactions. In Sec. III, the electron correlation of  $\kappa$ -BEDT-TTF salts is investigated by exactly diagonalizing the derived model Hamiltonian. In Sec. IV, we discuss electronic properties of  $\kappa$ -BEDT-TTF salts using the 2-D extended Hubbard model with different ranges of long-range Coulomb interactions with the HF approximation. The conclusion is given in Sec. V.

## II. AB INITIO MO STUDY OF ELECTRONIC AND GEOMETRICAL BEDT-TTF CLUSTERS

### A. *Ab initio* MO calculation

In Fig. 1, we show two stable conformations of the BEDT-TTF molecule, i.e., the staggered and eclipsed ones. As discussed by Demiralp and Goddard, the eclipsed one is slightly lower in energy and is chosen for *ab initio* calcula-

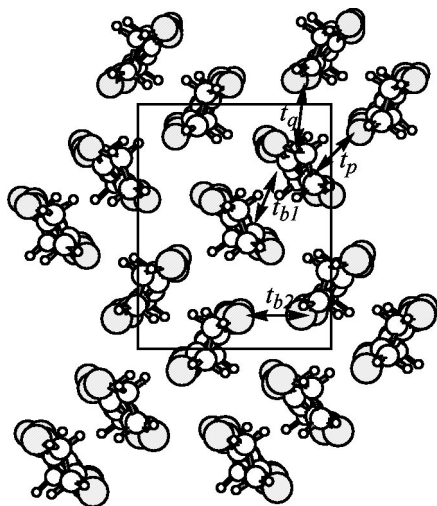
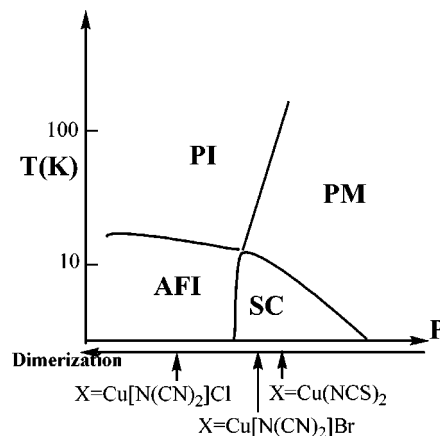
FIG. 2. Structure of the  $\kappa$ -phase BEDT-TTF conducting layer and definitions of transfer integrals.

FIG. 3. Experimental phase diagram of  $\kappa$ -(BEDT-TTF)<sub>2</sub>X as a function of pressure ( $P$ ) and temperature ( $T$ ). Here, PM, AFI, PI, and SC denote paramagnetic metal, antiferromagnetic insulator, paramagnetic insulator, and superconductor, respectively.

tions throughout this paper. We optimize the geometrical structure of BEDT-TTF at HF/double zeta plus polarization (DZP)<sup>28</sup> with a set of coupling coefficients for the formal charge,  $q = +1/2$ .<sup>29</sup>

A model Hamiltonian is constructed on the basis of calculations of BEDT-TTF clusters, the dimer, and a few tetramers. In all the calculations, the basis set is 31G valence functions with the Stevens–Basch–Krauss–Jasien (SBK) effective core potential (SBK-31G).<sup>30</sup> In the dimer calculation, the original basis functions are augmented by  $d$ -polarization functions for nonhydrogen atoms (SBK-31G\*). The formal charges are +1 and 0 for the dimer and tetramers, respectively. We freeze all atoms except hydrogen atoms at the locations determined by the x-ray diffraction (XRD) experiment<sup>3</sup> and optimize the locations of hydrogen atoms in the dimer unit at HF/SBK-31G.

To construct the model Hamiltonian, we obtain highest occupied molecular orbitals (HOMO) 1–2 for the dimer and HOMO 1–4 for the tetramers and localize them on each BEDT-TTF molecule following the Boys localization procedure.<sup>31</sup> Here, HOMO is spatial orbitals referred to neutral species. We evaluate transfer integrals in two different manners,  $t(1)$  and  $t(2)$ , based on the dimer calculation. Henceforth, the orbital indices,  $a, b, \dots$ ,  $\lambda, \dots$ , and  $p, q, \dots$ , denote doubly occupied, localized (LMO) and general molecular orbitals, respectively. The transfer integral,  $t(1)$ , is defined as half of the energy difference between the ground and first excited states, i.e.,  ${}^2A_u$  and  ${}^2A_g$  in the  $C_i$  frame. This convention was employed in the previous study of the DC-NQI salts.<sup>24</sup> The transfer integral,  $t(2)$ , is defined as

$$t(2) = \langle \lambda_1 | \tilde{f} | \lambda_2 \rangle, \quad (2.1)$$

where  $\lambda_1$  and  $\lambda_2$  are LMOs located on the first and second BEDT-TTF molecules, and the operator  $\tilde{f}$  is given by

$$\langle p | \tilde{f} | q \rangle = \langle p | h | q \rangle + \sum_{a \neq \text{HOMO}1-2} [2 \langle ap | aq \rangle - \langle ap | qa \rangle]. \quad (2.2)$$

The one- and two-electron integrals are

TABLE I. Structural parameters of BEDT-TTF<sup>+1/2</sup> from the HF/DZP calculations.

	Theory present	Theory <sup>a</sup>	Expt. <sup>2b</sup>
Distance			
$R(C_1-C_1)$	1.355	1.358	1.360
$R(C_1-S_1)$	1.746	1.747	1.741
$R(S_1-C_2)$	1.758	1.761	1.751
$R(C_2-C_2)$	1.333	1.329	1.343
$R(C_2-S_2)$	1.763	1.767	1.749
$R(S_2-C_3)$	1.811	1.814	1.811
$R(C_3-C_3)$	1.527	1.524	(1.485)
Angle			
$\theta(C_1-C_1-S_1)$	122.9	123.0	122.4
$\theta(C_1-S_1-C_2)$	95.9	96.0	95.1
$\theta(S_1-C_2-C_2)$	117.0	117.0	117.1
$\theta(C_2-C_2-S_2)$	128.7	128.8	128.9
$\theta(C_2-S_2-C_3)$	100.9	100.7	100.9
$\theta(S_2-C_3-C_3)$	113.0	112.8	(115.1)

<sup>a</sup>Averaged structural parameters of ET and ET<sup>+</sup> (Ref. 6).

<sup>b</sup> $\kappa$ -(BEDT-TTF)<sub>2</sub>Cu[N(CN)<sub>2</sub>]Br (Ref. 3).

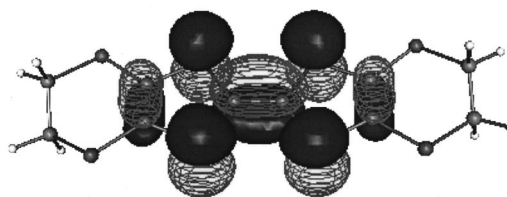
$$\langle p|h|q\rangle = \int dr_1 \varphi_p^*(r_1)h(r_1)\varphi_q(r_1), \quad (2.3)$$

$$\langle pq|rs\rangle = \int dr_1 dr_2 X\varphi_p^*(r_1)\varphi_q^*(r_2)r_{12}^{-1}\varphi_r(r_1)\varphi_s(r_2), \quad (2.4)$$

where  $h(r)$  is the one-electron Hamiltonian and  $\varphi(r)$  is the spatial orbital. On-site and nearest-neighbor Coulomb interactions,  $\langle \lambda_1\lambda_1|\lambda_1\lambda_1\rangle$  and  $\langle \lambda_1\lambda_2|\lambda_1\lambda_2\rangle$ , are estimated from the dimer calculations; other long-range interactions are determined from the tetramer ones. All of the calculations are performed with the GAMESS<sup>32</sup> and GAUSSIAN<sup>33</sup> suites of program packages.

## B. Geometrical structure of BEDT-TTF

In the  $\kappa$ -(BEDT-TTF)<sub>2</sub>[N(CN)<sub>2</sub>]X (X=Cl, Br, and I) crystals, each BEDT-TTF molecule has +1/2 charge according to their 3/4 filling. The optimized structural parameters of the BEDT-TTF<sup>+1/2</sup> monomer are shown in Table I. We also show the XRD parameters of  $\kappa$ -(BEDT-TTF)<sub>2</sub>[Cu(CN)<sub>2</sub>]Br at 127 K (Ref. 3) along with other averaged parameters of BEDT-TTF and BEDT-TTF<sup>+</sup> calculated by Demiralp and Goddard at HF/6-31G\*\*.<sup>6</sup> Definitions of the carbon and sulfur sites are depicted in Fig. 1. We see that the deviations of our results from the XRD parameters are within 0.02 Å and 0.5 deg in bond lengths and angles, respectively, except for  $R(C_3-C_3)$  and  $\theta(S_2-C_3-C_3)$ . Two reasons are considered for the deviations. One is the effect of neglecting the anion layer. The other is that the XRD structural parameters of the -CH<sub>2</sub>-CH<sub>2</sub>- group have an ambiguity since BEDT-TTF molecules can take both the staggered and eclipsed conformations as shown in Fig. 1. Demiralp and Goddard showed the energy difference between the conformations is very small, i.e., 0.0032 kcal/mol at HF/6-31G\*\* and suggested

FIG. 4. HOMO of the BEDT-TTF molecule at HF/DZP with  $q = +1$ .

the possibility that BEDT-TTF molecule can take both structures even at 10 K.<sup>7</sup> Our optimized structure also agrees with their calculation.

## C. HOMO and ionization potential

The calculated HOMO of the BEDT-TTF molecule is drawn in Fig. 4. The structural parameters used are taken from the XRD experiment of  $\kappa$ -(BEDT-TTF)<sub>2</sub>[N(CN)<sub>2</sub>]Br.<sup>3</sup> The antibonding character of -S<sub>1</sub>-C<sub>1</sub>- and -S<sub>1</sub>-C<sub>2</sub>- and bonding character of -C<sub>1</sub>-C<sub>1</sub>- and -C<sub>2</sub>-C<sub>2</sub>- are observed in HOMO. The HOMO coefficients of  $p$ -type orbitals in -C<sub>1</sub>-S<sub>1</sub>-C<sub>2</sub>- are large, whereas those of -S<sub>2</sub>-C<sub>3</sub>- are small. In the crystal, the formal charge of BEDT-TTF is +1/2 and the  $p$ -type orbitals of -C<sub>1</sub>-S<sub>1</sub>-C<sub>2</sub>- contribute to the conductivity of BEDT-TTF crystals.

The calculated vertical and adiabatic ionization potentials (IPs) are shown in Table II, where IP(1) and IP(2) denote those from the Koopmans theorem and from the  $\Delta$  self-consistent field (SCF) method, respectively. Our vertical IP(1) is overestimated, compared with the experimental one, 6.21 eV,<sup>34</sup> since the orbital relaxation is neglected in IP(1). On the other hand, the vertical and adiabatic IPs(2) are underestimated. The dependence of the basis set is small in both IPs.

## D. Transfer integrals and Coulomb interactions

In Table III, we show transfer integrals and Coulomb interactions derived from the dimer and tetramer calculations with  $q = +0$ . The transfer integrals are defined in Fig. 2. The sign of transfer integral,  $t(2)$ , depends on taking phases of wave function. For  $\kappa$ -(BEDT-TTF)<sub>2</sub>Cu[N(CN)<sub>2</sub>]Cl, on-site and nearest-neighbor Coulomb interactions are calculated to be 5.90 and 3.25 eV, respectively. These Coulomb interactions are bare and larger than the effective ones.<sup>11-13</sup>  $t_{b1}(1)$

TABLE II. Ionization potential from the HF calculations.

	IPV <sup>a</sup>	IPA <sup>b</sup>
IP(1) at HF/DZP	6.82	
IP(1) at HF/SBK-31G*	6.83	
IP(1) <sup>c</sup>	6.87	
IP(2) at HF/DZP	6.11	5.83
IP(2) at HF/SBK-31G*	6.15	5.82
IP(2) <sup>c</sup>		5.77
Experiment <sup>d</sup>		6.21

<sup>a</sup>Vertical ionization potential (eV).

<sup>b</sup>Adiabatic ionization potential (eV).

<sup>c</sup>Reference 6.

<sup>d</sup>Reference 34.

TABLE III. Transfer integrals and Coulomb interactions (eV) for (BEDT-TTF)<sub>2</sub>Cu[(CN)<sub>2</sub>]X (X=Cl, Br, I) from the HF/SBK-31G\* (dimer) and HF/SBK-31G (tetramer) calculations.

	Charge (tetramer)	Temperature	On-site Coulomb	Nearest- neighboring Coulomb	$t_{b1}(1)$ (eV)	$t_{b1}(2)$ (eV)	$t_{b2}(2)$ (eV)	$t_p(2)$ (eV)	$t_q(2)$ (eV)
(ET) <sub>2</sub> Cu[N(CN) <sub>2</sub> Cl]	+0	127 K	5.9004	3.2503	0.2743	0.2804	0.0717	-0.1584	-0.0319
(ET) <sub>2</sub> Cu[N(CN) <sub>2</sub> Br]	+0	127 K	5.9025	3.2270	0.2657	0.2687	0.0643	-0.1669	-0.0260
(ET) <sub>2</sub> Cu[N(CN) <sub>2</sub> I]	+0	127 K	5.8346	3.2198	0.2392	0.2438	0.0484	0.1610	-0.0162
(ET) <sub>2</sub> Cu[N(CN) <sub>2</sub> I]	+0	295 K	5.8332	3.1913	0.2328	0.2362	0.0513	-0.1480	-0.0235
(ET) <sub>2</sub> Cu[N(CN) <sub>2</sub> Br] <sup>a</sup>		127 K				-0.301	-0.080	-0.135	-0.047
(ET) <sub>2</sub> Cu[N(CN) <sub>2</sub> Br] <sup>b</sup>		RT <sup>c</sup>				0.244	0.092	0.101	-0.034

<sup>a</sup> $q_d=0$ , HF level (Ref. 16).

<sup>b</sup>Extend Hückel approximation (Ref. 35).

<sup>c</sup>Room temperature.

and  $t_{b1}(2)$  are calculated to be 0.274 and 0.280 eV, respectively. The difference is small, so that the orbital relaxation hardly affects the transfer integrals in the  $\kappa$ -(BEDT-TTF)<sub>2</sub>Cu[N(CN)<sub>2</sub>]X system. For X=Cl and Br,  $t_{b1}(1)$  are 0.274 and 0.266 eV, respectively. This ordering indicates the strength of dimerization, which is consistent with Kanoda's diagram in Fig. 3. Basically, our transfer integrals are consistent with the previous results of Fortunelli and Painelli at HF/6-31G\*\*.<sup>16</sup> However, the *ab initio* transfer integral,  $t_p(2) = -0.1584$  eV for X=Br is larger than the semiempirical one,  $-0.101$  eV, obtained from the extended Hückel calculation.<sup>35</sup>  $t_{b2}$  is a little smaller than the semiempirical one.

### E. Fermi surface and band dispersion

Within the tight-binding approximation, we calculate band dispersions and Fermi surfaces for X=Cl and Br using the three transfer integrals,  $t_{b1}(2)$ ,  $t_{b2}(2)$ , and  $t_p(2)$ . The  $t_{b1}(2)$  are the off-diagonal one-electron matrix elements between the two localized orbitals in the dimer calculation with  $q = +0$ , while the  $t_{b2}(2)$  and  $t_p(2)$  are those between the corresponding two localized orbitals in the tetramer calculations with  $q = +0$ . The results are shown in Figs. 5 and 6. The gap between the upper (antibonding) two bands and the lower (bonding) two bands of X=Cl is larger than that of X=Br. The calculated Fermi surface of X=Br is very similar to that of X=Cl. Our theoretical Fermi surface is consistent with the experimental one for the  $\kappa$ -(BEDT-TTF)<sub>2</sub>Cu[N(CN)<sub>2</sub>]Cl salt obtained by the angle-dependent magnetoresistance oscillation (ARMO) and

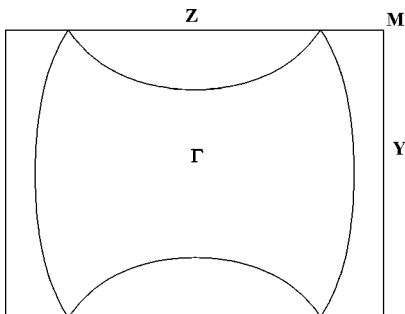


FIG. 5. Fermi surface of  $\kappa$ -(BEDT-TTF)<sub>2</sub>Cu[N(CN)<sub>2</sub>]Cl.

Shubnikov-de Haas oscillation experiments under pressure.<sup>36</sup> We find that the ratio of the closed part around the Z point in the Fermi surface is 20.7% for the  $\kappa$ -(BEDT-TTF)<sub>2</sub>Cu[N(CN)<sub>2</sub>]Cl salt, which is close to the experimental one, 16%–18%.<sup>37,38</sup> The Fermi surface and band dispersion are also consistent with first-principles ones calculated by Xu *et al.* based on LDA.<sup>5</sup> On the other hand, the ratio is calculated to be 26.2% with the semiempirical transfer integrals.<sup>35</sup>

### III. EXACT DIAGONALIZATION STUDY OF MODEL HAMILTONIAN

There are three electrons per dimer so that the upper molecular orbital (UMO) is half-filled. Therefore, the electronic properties mainly depend on the UMOs. To elucidate the effect of electron correlation, we employ a model Hamiltonian over the UMOs,

$$H_U = \sum_{\substack{m,n(m \neq n) \\ \sigma}} t_{mn} a_{m\sigma}^+ \alpha_{n\sigma} + \sum_m \langle mm|mm \rangle n_{m\uparrow} n_{m\downarrow} + \frac{1}{2} \sum_{m,n(m \neq n)} \langle mn|mn \rangle n_m n_n, \quad (3.1)$$

where the indices  $m, n, \dots$ , and  $\sigma$  denote UMOs and spins,  $n_{p\sigma} = a_{p\sigma}^+ a_{p\sigma}$  and  $n_p = a_{p\uparrow}^+ a_{p\uparrow} + a_{p\downarrow}^+ a_{p\downarrow}$ . The UMO  $|m\rangle$  is defined by

$$|m\rangle = \frac{1}{\sqrt{2}} [|\lambda_1\rangle - |\lambda_2\rangle], \quad (3.2)$$

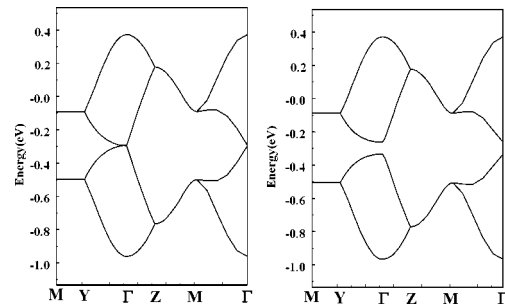


FIG. 6. Calculated band structures of X=Br (left) and X=Cl (right).

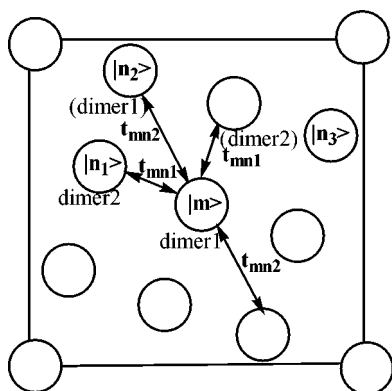


FIG. 7. BEDT-TTF decamer model.

where both of  $\lambda_{1-2}$  belong to one and the same dimer. One- and two-electron interactions over UMOs are calculated by transforming the HF integrals for the  $\kappa$ -(BEDT-TTF)<sub>2</sub>Cu[N(CN)<sub>2</sub>]Br salt at 127 K.<sup>3</sup> In this particular work, we use two different model Hamiltonians,  $H_{U1}$  and  $H_{U2}$ . These Hamiltonians include the same one-electron interactions and include the two-electron interactions up to the nearest-neighbor and next-nearest-neighbor dimers, respectively. The off-diagonal one-electron interaction is estimated from the half of the energy difference between the first and second HOMO orbital energies in the tetramer calculation with  $q = +0$ . The one-electron interactions,  $t_{mn_1}$  and  $t_{mn_2}$ , defined in Fig. 7 are calculated to be  $-0.114$  and  $-0.045$  eV, respectively. The two-electron interactions, on-site and long-range Coulomb interactions, are estimated from the UMOs [Eq. (3.2)] obtained by the dimer and tetramer calculations with  $q = +0$ . The values of the  $\langle mn|mm\rangle$ ,  $\langle mn_1|mn_1\rangle$ ,  $\langle mn_2|mn_2\rangle$ , and  $\langle mn_3|mn_3\rangle$  are 4.55, 1.88, 1.65, and 1.14 eV, respectively. The periodic boundary condition is used for the decamer model shown in Fig. 7. We employ the Slater-determinant-based direct configuration interaction (CI) method for diagonalizing the model Hamiltonians.<sup>39</sup>

We calculate the ground state of  $H_{U1}$  and analyze its spin-correlation function,

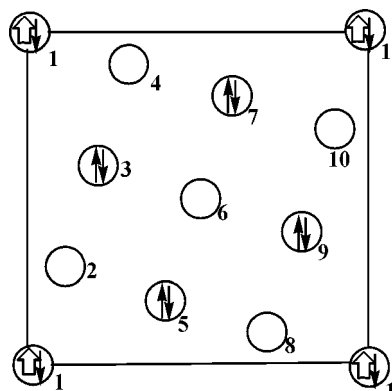


FIG. 8. Spin configuration in the ground state of  $H_{U1}$ . Arrows pointing upwards (downwards) represent up (down) spins. The solid arrows pointing  $\sigma$  at site  $j$  indicate that the spin-correlation function (3.3)  $\Delta_{1\uparrow,j\sigma}$  has a strong amplitude.

$$\Delta_{p\sigma,q\sigma'} = \langle n_{p\sigma} n_{q\sigma'} \rangle / N^2, \quad (3.3)$$

where  $N = \langle n_{p\sigma} \rangle$ . The ground state has charge ordering (CO) correlation as drawn in Fig. 8. The spin correlation functions,  $\Delta_{1\uparrow,m\uparrow}$  ( $m = 3, 5, 7, 9$ ) and  $\Delta_{1\uparrow,m\downarrow}$  ( $m = 1, 3, 5, 7, 9$ ), are 2.00. Other  $\Delta_{1\uparrow,m\sigma}$  are less than 0.01. This implies that the localization is strong. On the other hand, the ground state of  $H_{U2}$ , has the antiferromagnetic (AF) correlation as drawn in Fig. 9. The spin-correlation functions,  $\Delta_{1\uparrow,m\uparrow}$  ( $m = 3, 5, 7, 9$ ) and  $\Delta_{1\uparrow,6\downarrow}$  are close to 1.30 and  $\Delta_{1\uparrow,m\downarrow}$  ( $m = 2, 4, 8, 10$ ) are close to 1.47. The other  $\Delta_{1\uparrow,m\sigma}$  are less than 0.75. This ordering is consistent with the experimental one.<sup>40</sup> These results indicate that the next-nearest-neighbor Coulomb interactions are important to reproduce the AF ordering correctly.

#### IV. THE HF STUDY OF THE 2-D EXTENDED HUBBARD MODEL

##### A. The 2-D extended Hubbard model within the HF approximation

To clarify the effects of the long-range Coulomb interactions in the  $\kappa$ -BEDT-TTF salts, we introduce a 2-D extended Hubbard model by extracting their 2-D conducting plane and neglecting their anion layers. The indices,  $i, j, \dots$ , denote HOMOs localized on the BEDT-TTF molecules. The Hamiltonian is defined by

$$H = \sum_{i,j,\sigma} t_{ij} a_{i\sigma}^+ a_{j\sigma} + \sum_i U n_{i\uparrow} n_{i\downarrow} + \sum_{i \neq j} V_{ij} n_i n_j, \quad (4.1)$$

where  $t_{ij}$ ,  $V_{ij}$ , and  $U$  denote transfer integral and Coulomb interactions between  $i$  and  $j$  sites, and on-site Coulomb interaction, respectively. In this Hamiltonian, we use the one- and two-electron interactions calculated for the  $\kappa$ -(BEDT-TTF)<sub>2</sub>Cu[N(CN)<sub>2</sub>]Br salt at 127 K. The transfer integrals,  $t_{b1}(2)$ ,  $t_{b2}(2)$ , and  $t_p(2)$ , and on-site Coulomb interaction in Table III are used and  $t_q(2)$  is neglected. We include Coulomb interaction,  $V_{ij}$ , up to the next-nearest-neighbor dimer as shown in Fig. 10. These parameters are shown in Table IV. The Coulomb interactions,  $V_{13}$  and  $V_{27}$ , are referred to as  $V_{NN}$  and  $V_{NNN}$ , respectively. The unit cell includes four BEDT-TTF molecules, that is, two dimers as shown in Fig. 11. We fix the ratios among the nearest-neighbor interactions, i.e.,  $V_{14}/V_{13}$ ,  $V_{15}/V_{13}$ , and  $V_{16}/V_{13}$ , and the ones among the next-nearest-neighbor interactions,

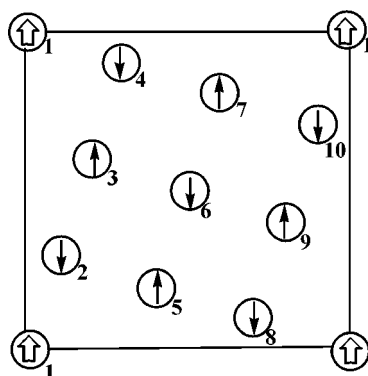


FIG. 9. Spin configuration in the ground state of  $H_{U2}$ . The meaning of the arrows is the same as in Fig. 9.

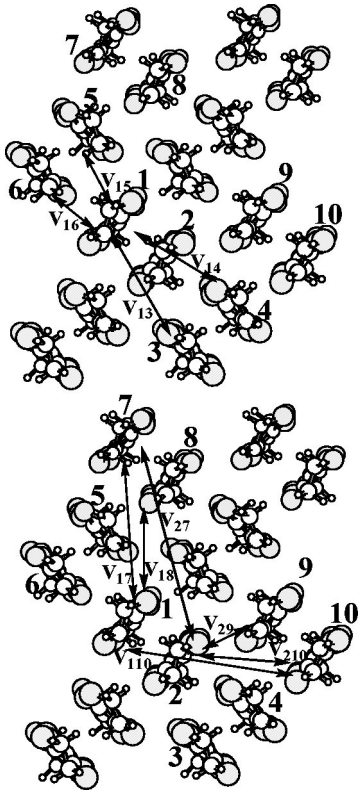


FIG. 10. Nearest-neighbor Coulomb interactions (top) and next-nearest-neighbor Coulomb interactions (bottom).

i.e.,  $V_{29}/V_{27}$ ,  $V_{210}/V_{27}$ ,  $V_{17}/V_{27}$ ,  $V_{18}/V_{27}$ , and  $V_{110}/V_{27}$  to elucidate the physical properties, regarding the BEDT-TTF dimer as a unit. The densities are determined self-consistently and the electron occupation is fixed to be six electrons in four molecules.

We apply the HF approximation,

$$Un_{i\uparrow}n_{i\downarrow} \approx U(\langle n_{i\uparrow} \rangle n_{i\downarrow} + n_{i\uparrow} \langle n_{i\downarrow} \rangle - \langle n_{i\uparrow} \rangle \langle n_{i\downarrow} \rangle), \quad (4.2)$$

$$\begin{aligned} V_{ij}n_in_j \approx & V_{ij}(\langle n_i \rangle n_j + n_i \langle n_j \rangle - \langle n_i \rangle \langle n_j \rangle) \\ & - \langle a_{i\uparrow}^+ a_{j\uparrow} \rangle a_{j\uparrow}^+ a_{i\uparrow} - a_{i\uparrow}^+ a_{j\uparrow} \langle a_{j\uparrow}^+ a_{i\uparrow} \rangle \\ & + \langle a_{i\uparrow}^+ a_{j\uparrow} \rangle \langle a_{j\uparrow}^+ a_{i\uparrow} \rangle - \langle a_{i\downarrow}^+ a_{j\downarrow} \rangle a_{j\downarrow}^+ a_{i\downarrow} \\ & - a_{i\downarrow}^+ a_{j\downarrow} \langle a_{j\downarrow}^+ a_{i\downarrow} \rangle + \langle a_{i\downarrow}^+ a_{j\downarrow} \rangle \langle a_{j\downarrow}^+ a_{i\downarrow} \rangle. \end{aligned} \quad (4.3)$$

TABLE IV. Coulomb interactions of  $\kappa$ -(BEDT-TTF)<sub>2</sub>Cu[N(CN)<sub>2</sub>]X (X=Cl, Br, I) salts at HF/SBK-31G (eV).

	X=Cl	X=Br	X=I
$V_{16}$	2.428	2.441	2.409
$V_{13}$	1.428	1.419	1.438
$V_{14}$	1.529	1.528	1.520
$V_{15}$	2.160	2.164	2.177
$V_{29}$	2.139	2.113	2.071
$V_{210}$	1.640	1.629	1.592
$V_{110}$	1.247	1.238	1.216
$V_{18}$	1.389	1.406	1.408
$V_{17}$	1.118	1.121	1.136
$V_{27}$	0.909	0.905	0.923

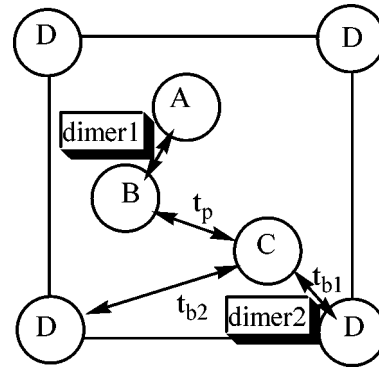


FIG. 11. Model of  $\kappa$ -(BEDT-TTF)<sub>2</sub>Cu[N(CN)<sub>2</sub>]X. The circles represent BEDT-TTF molecules.

The ground state of the Hamiltonian is calculated using  $20 \times 30$   $k$ -points on the  $a^* \times c^*$  conducting plane in the momentum space. The electron densities are given by

$$n_{i\sigma} = \frac{1}{N_{\text{cell}}} \sum_a \sum_k^{\text{occ}} c_{kai\sigma}^* c_{kai\sigma}, \quad (4.4)$$

where  $N_{\text{cell}}$  represents the total number of cells and the coefficient of the  $a$ th eigenvector of  $i$ th site at  $k$  point in the Brillouin zone is written as  $c_{kai\sigma}$ .

### B. Effects of Coulomb interactions on electronic states

Since Kino and Fukuyama have already discussed the effect of the intradimer transfer integral,  $t_{b1}$ , based on the HF model,<sup>12</sup> we fix the *ab initio* transfer integrals and concentrate on the role of Coulomb interactions.

We first study the effect of on-site Coulomb interaction,  $U$ , changing  $U$  as a variable from 0 to 1.2 eV and neglecting  $V_{ij}$ . In Fig. 12, the absolute value of spin moment per molecule,  $\langle S_z \rangle$ , is drawn as a function of  $U$ . In the region,  $0 < U < 0.7$  eV, the ground state is a paramagnetic metal. The hole density ( $\rho_h$ ) is close to +0.5 at each site. In the region,  $0.7 < U < 0.95$  eV, the HF calculations did not converge due to quasidegeneracy. At  $U = 0.95$  eV, the system becomes an AF insulator. The configuration of spin alignments with  $S_z(A) = S_z(B)$  and  $S_z(C) = S_z(D)$  is shown in the inset of Fig. 12. Since the direction of the spin moment of dimer 1 and that of dimer 2 are opposite, the AF ordering occurs between dimers.  $\rho_h$  is close to +0.5 at each site. The spin moment becomes about  $0.4\mu_B$  per BEDT-TTF molecule. This magnitude of spin moment agrees with the experimentally observed one in the AF ordered state,  $0.4\text{--}1.0\mu_B$  per

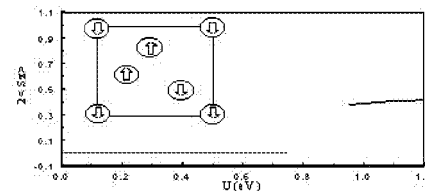


FIG. 12.  $U$  dependence of magnetic moment  $\langle S_z \rangle$ . The inset shows the alignment of spin moments. Arrows pointing upwards (downwards) represent up (down) spins.

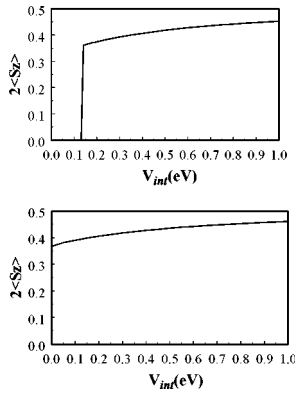


FIG. 13.  $V_{\text{int}}$  dependence of magnetic moment  $\langle S_z \rangle$ . Here, the top figure is for  $U=0.7$  eV, whereas the bottom one is for  $U=0.9$  eV.

dimer.<sup>40</sup> As  $U$  increases, the spin moment becomes large and finally saturated. These results are consistent with the previous results by Kino and Fukuyama,<sup>12</sup> and Demiralp and Goddard,<sup>9</sup> who also applied the HF approximation to the 2-D Hubbard model of the  $\kappa$ -(BEDT-TTF)<sub>2</sub>Cu(NCS)<sub>2</sub> salt.

Then, we change the intradimer Coulomb interaction,  $V_{\text{int}}$ , from 0 to 1.0 eV for  $U=0.7$  and 0.9 eV. The absolute value of spin moment per molecule,  $\langle S_z \rangle$ , is shown as a function of  $V_{\text{int}}$  in Fig. 13. In the case of  $U=0.9$  eV, the ground state is an AF insulator in the entire range,  $0 < V_{\text{int}} < 1.0$  eV. The AF spin configuration is almost the same as in Fig. 12. The magnitude of spin moment increases slightly as  $V_{\text{int}}$  becomes larger. At  $U=0.7$  eV, the ground state is the paramagnetic metal for  $0 < V_{\text{int}} < 0.14$  eV. However, when  $V_{\text{int}}=0.14$  eV, the AF insulator has a lower energy. We check the contribution of transfer integrals,  $U$  and  $V_{\text{int}}$ , to the HF total energies. The Fock term of  $V_{\text{int}}$  is found to mainly stabilize an AF insulator.

Using the isolated dimer model, we evaluate the effective on-site Coulomb interaction on the dimer,  $U_{\text{dimer}}$ , defined as  $E(2)+E(0)-2E(1)$ , where  $E(n)$  is the total energy of the dimer with  $n$  electron(s). We derive the total energy of the Hamiltonian,

$$H = \varepsilon \sum_{i,\sigma}^2 a_{i\sigma}^+ a_{i\sigma} - t_{b1} \sum_{\sigma} (a_{1\sigma}^+ a_{2\sigma} + a_{2\sigma}^+ a_{1\sigma}) + \sum_i^2 (U n_{i\uparrow} n_{i\downarrow} + V_{\text{int}} n_{1\uparrow} n_{2\downarrow}), \quad (4.5)$$

considering all spin configurations where  $\varepsilon$  is the orbital energy of BEDT-TTF HOMO. The indices, 1 and 2, represent different BEDT-TTF molecules in the dimer. The total energies of the lowest states with 1 and 2 electrons and  $U_{\text{dimer}}$  are given by

$$E(2) = 2\varepsilon + \frac{1}{2}(U + V_{\text{int}}) - \frac{1}{2}(U - V_{\text{int}}) \sqrt{1 + \left(\frac{4t_{b1}}{U - V_{\text{int}}}\right)^2}, \quad (4.6)$$

$$E(1) = \varepsilon - t_{b1}, \quad (4.7)$$

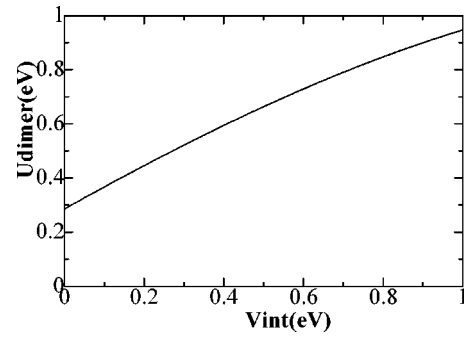


FIG. 14.  $V_{\text{int}}$  dependence of  $U_{\text{dimer}}$  with  $U=0.9$  eV.

$$U_{\text{dimer}} = E(2) + E(0) - 2E(1)$$

$$= 2t_{b1} + \frac{1}{2}(U + V_{\text{int}}) - \frac{1}{2}(U - V_{\text{int}}) \sqrt{1 + \left(\frac{4t_{b1}}{U - V_{\text{int}}}\right)^2}. \quad (4.8)$$

$U_{\text{dimer}}$  are calculated to be 0.29 and 0.66 eV for two sets of parameters,  $V_{\text{int}}=0$  eV,  $U=0.9$  eV and  $V_{\text{int}}=0.5$  eV,  $U=0.9$  eV, respectively. We show  $U_{\text{dimer}}$  as a function of  $V_{\text{int}}$  in Fig. 14. This indicates that  $V_{\text{int}}$  enhances  $U_{\text{dimer}}$  and supports our HF results.

Next, we inspect the nearest-neighbor Coulomb interaction,  $V_{\text{NN}}$ . The value of charge disproportionation,  $\delta$  (deviation from the average value, 1.5) and the magnitude of spin moment per molecule,  $\langle S_z \rangle$ , as functions of  $V_{\text{NN}}$  are shown in Fig. 15. The parameter,  $V_{\text{NN}}$ , is changed from 0 to 0.5 eV with  $U=0.9$  eV and  $V_{\text{int}}=0.5$  eV. In the range of  $0 < V_{\text{NN}} < 0.14$  eV, the ground state is an AF insulator with spin moment,  $\sim 0.41\mu_B$ . At  $V_{\text{NN}}=0.14$  eV, the ground state becomes the CO [purely electronic charge-density wave (CDW)] state. The charge disproportionation  $\delta$  of A and B sites are 0.47, and those of C and D are  $-0.47$  at  $V_{\text{NN}}=0.2$  eV.

We change the two parameters, next-nearest-neighbor Coulomb interaction,  $V_{\text{NNN}}$ , and nearest-neighbor Coulomb interaction,  $V_{\text{NN}}$ , with  $U=0.9$  eV and  $V_{\text{int}}=0.5$  eV. The phase diagram of  $V_{\text{NN}}$  and  $V_{\text{NNN}}$  is shown in Fig. 16. In the range,  $0 < V_{\text{NN}} < 0.1$  eV and  $0 < V_{\text{NNN}} < 0.4$  eV, the ground

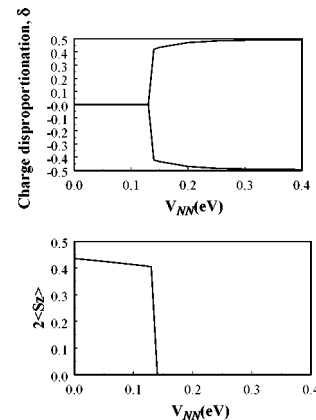


FIG. 15.  $V_{\text{NN}}$  dependence of magnetic moment  $\langle S_z \rangle$  (top) and charge disproportionation  $\delta$  (bottom) with  $U=0.9$  eV and  $V_{\text{int}}=0.5$  eV.

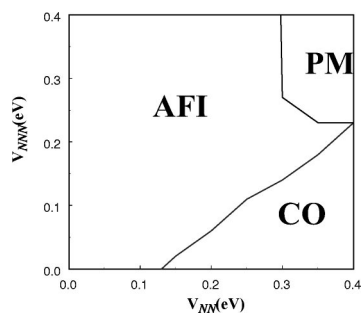


FIG. 16. Phase diagram as a function of  $V_{NN}$  and  $V_{NNN}$  with  $U=0.9$  eV and  $V_{int}=0.5$  eV. Here, AFI, PM, and CO represent the antiferromagnetic insulator, paramagnetic metal, and charge ordering states, respectively.

state is the AF insulator. At  $V_{NN}=0.15$  eV and  $V_{NNN}=0$  eV, the CO state has a lower energy. In the range,  $0.3 < V_{NN} < 0.4$  eV and  $0.3 < V_{NNN} < 0.4$  eV, the ground state is a paramagnetic metal. Since the unit cell includes only two BEDT-TTF dimers, we cannot describe the orderings whose periodicities are larger than that of the unit cell, though other ordering states might have lower energies. However, Poilblanc *et al.* calculated the ground state of the 1-D extended Hubbard model by the exact diagonalization method and also found that its ground state is the paramagnetic metal in a certain range of Coulomb interactions<sup>41</sup> similar to the present case.

As was shown in Sec. III, the dimer model offers a reasonable description of the  $\kappa$ -BEDT-TTF salts. Based upon this fact, we employ infinite half-filled square-lattice models to approximate the 2-D extended Hubbard model at strong coupling,

$$H = \sum_i U n_{i\uparrow} n_{i\downarrow} + \sum_{i,j \in \text{NNsite}} V_1 n_i n_j + \sum_{i,j \in \text{NNNsite}} V_2 n_i n_j, \quad (4.9)$$

where NNsite and NNNsite represent the nearest-neighbor and next-nearest-neighbor sites, respectively, and  $U$ ,  $V_1$ , and  $V_2$  are the on-site, nearest-neighbor, and next-nearest-neighbor Coulomb interactions, respectively. In this model, we neglect transfer integrals. Two spin configurations, which correspond to the obtained AF and CO states, are shown in Fig. 17. The unit cell is shown by the dashed line. Using Eq. (4.9), the energies per unit cell of both models are calculated to be  $4V_1 + 4V_2$  and  $U + 8V_2$ , respectively. The CO configuration is stabilized for  $V_1 > V_2 + U/4$ , whereas the AF spin configuration is more stable for  $V_1 < V_2 + U/4$ . Actually, as shown in the phase diagram, the ground state is the CO state in the range,  $V_{NN} > V_{NNN} + U/4$  and the ground state is the AF state in the range,  $V_{NN} < V_{NNN} < 0.2$ .

## V. CONCLUSION

We calculated the geometrical and electronic structures of a BEDT-TTF monomer at HF/DZP. The optimized structure reproduces the experimental one very well except for the  $-\text{CH}_2-\text{CH}_2-$  group. Transfer integrals and Coulomb interactions were calculated and compared with experimental and other theoretical results. Using *ab initio* transfer integrals, we calculated band dispersions and Fermi surfaces of

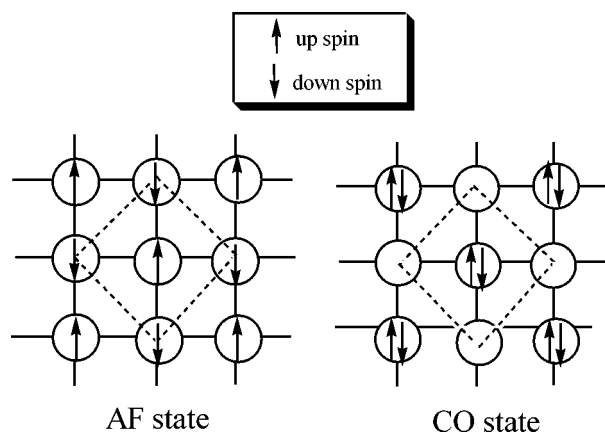


FIG. 17. Spin configuration in the antiferromagnetic (AF) and charge ordering (CO) states.

$\kappa$ -(BEDT-TTF)<sub>2</sub>Cu[N(CN)<sub>2</sub>]<sub>2</sub>X (X=Br, Cl). The exact diagonalization study of the derived model Hamiltonian shows that the ground state has AF correlation. This result is consistent with the experimental one. To study the role of long-range Coulomb interactions, we calculated the ground state of a 2-D extended Hubbard model within the HF approximation. Then, we found that the intradimer Coulomb interaction,  $V_{int}$ , enhances the effective on-site Coulomb interaction on the dimer ( $U_{dimer}$ ), which controls the transition between the paramagnetic metal and AF state. The phase diagram as a function of representative nearest-neighbor and next-nearest-neighbor Coulomb interactions,  $V_{NN}$  and  $V_{NNN}$ , was elucidated. It is found that the ground state shows various phases, i.e., AF, CO, and paramagnetic metal phases, controlled by the ratio of  $V_{NN}$  and  $V_{NNN}$ . When  $V_{NN}$  is larger than some critical value in the absence of  $V_{NNN}$ , the ground state is the CO state. On the other hand, when  $V_{NNN}$  is larger than  $V_{NN}$ , the ground state is the AF insulator or paramagnetic metal. Therefore, we conclude that it is necessary to consider enough ranges of long-range Coulomb interactions to calculate the electronic properties.

## ACKNOWLEDGMENTS

We acknowledge fruitful discussions with and useful suggestions by Professor Hayao Kobayashi and Professor Kazushi Kanoda. We also thank Dr. Michiyasu Mori for variable advices and programming assistance. One of the authors (Y.I.) is indebted for the JSPS Research Fellowship for Young Scientists. This work was partially supported by a Grant-in-Aid for JSPS Fellows from the Ministry of Education, Science, Sports, and Culture, Japan. The numerical calculations were performed at the computer center of Institute for Molecular Science.

<sup>1</sup>L. B. Coleman, M. J. Cohen, D. J. Sandman, F. F. Yamagishi, A. F. Garito, and A. J. Heeger, *Solid State Commun.* **12**, 1125 (1973).

<sup>2</sup>H. H. Wang, K. D. Carlson, U. Geiser, A. M. Kini, A. J. Schultz, J. M. Williams, L. K. Montgomery, W. K. Kwok, U. Welp, K. G. Vandervoort, S. J. Boryschuk, A. V. Strieby Crouch, J. M. Kommers, D. M. Watkins, J. E. Schirber, D. L. Overmyer, D. Jung, J. J. Novoa, and M.-H. Whangbo, *Synth. Met.* **42**, 1983 (1991).

<sup>3</sup>U. Geiser, A. J. Schultz, H. H. Wang, D. M. Watkins, D. L. Stupka, J. M.

- Williams, J. E. Schirber, D. L. Overmyer, D. Jung, J. J. Novoa, and M.-H. Whangbo, *Physica C* **174**, 475 (1991).
- <sup>4</sup>K. Kanoda, *Hyperfine Interact.* **104**, 235 (1997).
- <sup>5</sup>Y.-N. Xu, W. Y. Ching, Y. C. Jean, and Y. Lou, *Phys. Rev. B* **52**, 12946 (1995).
- <sup>6</sup>E. Demiralp and W. A. Goddard III, *J. Phys. Chem.* **98**, 9781 (1994).
- <sup>7</sup>E. Demiralp, S. Dasgupta, and W. A. Goddard III, *J. Am. Chem. Soc.* **117**, 8154 (1995).
- <sup>8</sup>E. Demiralp, S. Dasgupta, and W. A. Goddard III, *J. Phys. Chem. A* **101**, 1975 (1997).
- <sup>9</sup>E. Demiralp and W. A. Goddard III, *Phys. Rev. B* **56**, 11907 (1997).
- <sup>10</sup>E. Demiralp and W. A. Goddard III, *J. Phys. Chem. A* **102**, 2466 (1998).
- <sup>11</sup>H. Kino and H. Fukuyama, *J. Phys. Soc. Jpn.* **64**, 1877 (1995).
- <sup>12</sup>H. Kino and H. Fukuyama, *J. Phys. Soc. Jpn.* **64**, 2726 (1995).
- <sup>13</sup>H. Kino and H. Fukuyama, *J. Phys. Soc. Jpn.* **64**, 4523 (1995).
- <sup>14</sup>A. Fortunelli and A. Painelli, *J. Chem. Phys.* **106**, 8041 (1997).
- <sup>15</sup>A. Fortunelli and A. Painelli, *J. Chem. Phys.* **106**, 8051 (1997).
- <sup>16</sup>A. Fortunelli and A. Painelli, *Phys. Rev. B* **55**, 16088 (1997).
- <sup>17</sup>G. Visentini, A. Painelli, A. Girlando, and A. Fortunelli, *Europhys. Lett.* **42**, 467 (1998).
- <sup>18</sup>Y. Okuno and H. Fukutome, *Solid State Commun.* **101**, 355 (1997).
- <sup>19</sup>C. E. Campos, P. S. Sandhu, J. S. Brooks, and T. Ziman, *Phys. Rev. B* **53**, 12725 (1996).
- <sup>20</sup>M. Gusmao and T. Ziman, *Phys. Rev. B* **54**, 16663 (1996).
- <sup>21</sup>H. Kino and H. Kontani, *J. Phys. Soc. Jpn.* **67**, 3691 (1998).
- <sup>22</sup>H. Kondo and T. Moriya, *J. Phys. Soc. Jpn.* **67**, 3695 (1998).
- <sup>23</sup>J. Schmalian, *Phys. Rev. Lett.* **81**, 4232 (1998).
- <sup>24</sup>Y. Imamura, S. Ten-no, and Y. Tanimura, *J. Phys. Chem. B* **103**, 266 (1999).
- <sup>25</sup>Y. Imamura, S. Ten-no, K. Yonemitsu, and Y. Tanimura, *Chem. Phys. Lett.* **298**, 15 (1998).
- <sup>26</sup>H. Seo and H. Fukuyama, *J. Phys. Soc. Jpn.* **66**, 1249 (1997).
- <sup>27</sup>N. Kobayashi, M. Ogata, and K. Yonemitsu, *J. Phys. Soc. Jpn.* **67**, 1098 (1998).
- <sup>28</sup>T. H. Dunning, Jr. and P. J. Hay, in *Method of Electronic Structure Theory*, edited by H. F. Schaefer III (Plenum, New York, 1977).
- <sup>29</sup>The used coupling coefficients were  $f_1=1$ ,  $f_2=0.75$ ,  $\alpha_{11}=2$ ,  $\alpha_{12}=1.5$ ,  $\alpha_{22}=0.5$ ,  $\beta_{11}=-1$ ,  $\beta_{12}=-0.75$ ,  $\beta_{22}=0$  in the energy expression,  $E=2\sum_j f_j h_{ii} + \sum_{ij} \alpha_{ij} \langle ij|ij \rangle + \beta_{ij} \langle ij|ji \rangle$ , where the indices, 1 and 2, denote doubly occupied and 3/4-filled orbitals, respectively.
- <sup>30</sup>W. J. Stevens, H. Basch, and M. J. Krauss, *J. Chem. Phys.* **81**, 6026 (1984).
- <sup>31</sup>S. F. Boys, in *Quantum Science of Atoms, Molecules, and Solids*, edited by P. O. Lowdin (Academic, New York, 1966).
- <sup>32</sup>M. W. Schmidt, K. K. Baldrige, J. A. Boatz, S. T. Elbert, M. S. Gordon, J. H. Jensen, S. Koseki, N. Matsunaga, K. A. Nguyen, S. J. Su, T. L. Windus, M. Dupuis, and J. A. Montgomery, *J. Comput. Chem.* **14**, 1347 (1993).
- <sup>33</sup>M. J. Frisch, G. W. Trucks, H. B. Schlegel, P. M. W. Gill, B. G. Johnson, M. A. Robb, J. R. Cheeseman, T. A. Keith, G. A. Petersson, J. A. Montgomery, K. Raghavachari, M. A. Al-Laham, V. G. Zakrzewski, J. V. Ortiz, J. B. Foresman, C. Y. Peng, P. Y. Ayala, M. W. Wong, J. L. Andres, E. S. Replogle, R. Gomperts, R. L. Martin, D. J. Fox, J. S. Binkley, D. J. Defrees, J. Baker, J. P. Stewart, M. Head-Gordon, C. Gonzalez, and J. A. Pople, *GAUSSIAN 94*, Gaussian, Inc., Pittsburgh, PA, 1995.
- <sup>34</sup>N. Sato, G. Saito, and H. Inokuchi, *Chem. Phys.* **76**, 79 (1983).
- <sup>35</sup>T. Komatsu, N. Matsukawa, T. Inoue, and G. Saito, *J. Phys. Soc. Jpn.* **65**, 1340 (1996).
- <sup>36</sup>Y. Yamauchi, M. V. Kartsovnik, T. Ishiguro, M. Kubota, and G. Saito, *J. Phys. Soc. Jpn.* **65**, 354 (1996).
- <sup>37</sup>T. Sasaki, H. Sato, and N. Toyata, *Solid State Commun.* **76**, 507 (1990).
- <sup>38</sup>K. Oshima, T. Mori, H. Inokuchi, H. Urayama, H. Yamochi, and G. Saito, *Phys. Rev. B* **38**, 938 (1988).
- <sup>39</sup>P. J. Knowles and N. C. Handy, *Chem. Phys. Lett.* **111**, 315 (1984).
- <sup>40</sup>K. Miyagawa, A. Kawamoto, Y. Nakazawa, and K. Kanoda, *Phys. Rev. Lett.* **75**, 1174 (1995).
- <sup>41</sup>D. Poilblanc, S. Yunoki, S. Maekawa, and E. Dagotto, *Phys. Rev. B* **56**, R1645 (1997).